Accurate Quantum Dynamics on Grid Platforms: Some Effects of Long Range Interactions on the Reactivity of N + N_2

Sergio Rampino[1], Ernesto Garcia[2], Fernando Pirani[1], and Antonio Laganà[1]

[1] Università degli Studi di Perugia, Dipartimento di Chimica,
Via Elce di Sotto 8, 06123 Perugia, Italia
[2] Universidad del Pais Vasco, Departamento de Quimica Fisica,
Paseo de la Universidad 7, 01006 Vitoria, España

Abstract. The potential energy surface of the N + N_2 atom diatom system has been reformulated using the LAGROBO functional form for interpolating ab initio points in the short distance region and using a modified Lennard Jones functional form to model the van der Waals interaction at long range. On the proposed surface extended quantum calculations have been performed using the European Grid platform. The values of the calculated thermal rate coefficients fairly reproduce the experimental results.

Keywords: Reactive scattering, quantum dynamics and kinetics, nitrogen exchange reaction, state specific reaction probabilities, thermal rate coefficients.

1 Introduction

The exchange and dissociation reactions of the nitrogen atom - nitrogen molecule system play a primary role in the modeling of spacecraft reentry [1]. Both the heat load and the reactivity of the species produced by the shock wave are, in fact, important data for heat shield design since nitrogen is the major component of Earth's atmosphere. Reactions of nitrogen are also important in other high temperature environments involving N_2, as, for example, shock tube experiments [2]. Experimental measurements of the N + N_2 thermal rate coefficients are available at the temperatures of 3400 and 1273 K [3,4,5].

The significant progress made in the last decades in computing the properties of atom diatom exchange reactions using quantum means has made it possible to calculate related detailed reactive probabilities and (by properly averaging them) thermal rate coefficients. A crucial step of the theoretical study is the assemblage of an accurate potential energy surface (PES). For this reason in the recent past extended ab initio calculations led to the formulation of the WSHDSP [6] and the L4 [7] PESs. On both PESs extended quantum calculations have been performed to the end of evaluating the thermal rate coefficient at the temperature of the experiments. Unfortunately, calculated values differ orders of magnitude from available experimental data not confirming the claimed accuracy of the proposed PESs.

D. Taniar et al. (Eds.): ICCSA 2010, Part IV, LNCS 6019, pp. 1–12, 2010.

For this reason in the work reported here we exploit the flexibility of the LAGROBO (Largest Angle Generalization of the ROtating Bond Order) functional form [7,8,9] to lower the minimum energy profile of the L4 PES and we incorporate an accurate description of the atom diatom long range interaction. On the resulting PES (ML4LJ), a computational campaign has been carried out to calculate the thermal rate coefficients using the time independent quantum reactive scattering program ABC [10] implemented on the section of the production computing Grid of EGEE [11] accessible to the COMPCHEM [12] virtual organization.

Accordingly, the article is organized as follows. In Sect. 2, the reasons for reformulating the N_3 interaction are illustrated. In Sect. 3, the computational machinery is described. In Sect. 4, calculated values of the rate coefficient are compared to experimental data.

2 Modeling the Interaction

A LEPS PES was the first functional formulation of the interaction for the N + N_2 system to ever appear in the literature [13]. Such PES has a saddle to reaction associated with a symmetric collinear ($\widehat{\mathrm{NNN}} = 180°$) geometry. The ab initio finding of a bent ($\widehat{\mathrm{NNN}} \simeq 120°$) geometry at the saddle to reaction was reported first in Refs. [14,15]. This proved the inadequacy of the LEPS PES to describe correctly the main features of the strong interaction region of the reaction channel and motivated the development of a new functional representation of the PES called L3 and based on the LAGROBO formulation [16].

More recently new high-level ab initio calculations have been performed for three thousand geometries of the N + N_2 system [6], and calculated values have been fitted using the unpublished WSHDSP functional form. The WSHDSP PES exhibits the peculiar feature of leading to a minimum energy path showing two fairly high barriers sandwiching a shallow well. The same high level ab initio approach was followed by us to generate the L4 PES [7] based also on the LAGROBO functional form and having similar characteristics. The failure of quantum results to reproduce the measured values of the thermal rate coefficient prompted an extended analysis of the detailed state to state probabilities. The analysis showed that, despite the different reactivities of N + N_2 on the L4 and on the WSHDSP PES, on both surfaces the calculations underestimate the measured value of the rate coefficient mainly because of the same strong interaction region shape [17].

In this paper we describe the assemblage of the ML4LJ PES for which, following the suggestions of [14,15], we adopt a lower energy value for the minimum energy path in the strong interaction region and add a properly parametrized Lennard Jones tail in the long range region.

2.1 The LAGROBO Formulation

The procedure followed to lower the potential energy in the strong interaction region exploits the flexibility of the LAGROBO functional form (V^{LAGROBO})

adopted to formulate the already mentioned L4 PES. The LAGROBO functional form is, in fact, built out of a combination of the ROtating Bond Order (ROBO) [8] V_τ^{ROBO} model potentials associated with the description of the various (τ) exchange processes allowed for the considered system as follows:

$$V^{\mathrm{LAGROBO}}(r_{\tau,\tau+1}, r_{\tau+1,\tau+2}, r_{\tau+2,\tau}) = \sum_\tau w(\Phi_\tau) V_\tau^{\mathrm{ROBO}}(\rho_\tau, \alpha_\tau, \Phi_\tau) \ . \qquad (1)$$

In (1) $r_{\tau,\tau+1}$ is the internuclear distance of the $\tau, \tau+1$ diatom with $\tau = 1$ for the A + BC arrangement while ρ_τ and α_τ are the hyperradius and hyperangle of the hyperspherical BO (HYBO) coordinates defined as

$$\rho_\tau = (n_{\tau+2,\tau}^2 + n_{\tau,\tau+1}^2)^{1/2} \text{ and } \alpha_\tau = \arctan[n_{\tau,\tau+1}/n_{\tau+2,\tau}] \ . \qquad (2)$$

In (2) $n_{\tau,\tau+1} = \exp[-\beta_{\tau,\tau+1}(r_{\tau,\tau+1} - r_{\mathrm{eq}\tau,\tau+1})]$ is the BO coordinate of the $\tau, \tau+1$ diatom with the process index τ being cyclic of module 3 and indicating the exchanged atom. The weight function $w(\Phi_\tau)$ of (1) is such as to privilege the ROBO potential better representing the overall interaction as the related Φ_τ (the angle formed by the two (broken and formed) bonds having in common the atom τ) varies [16]. It is defined as

$$w(\Phi_\tau) = \frac{u(\Phi_\tau)}{\sum_\tau u(\Phi_\tau)} \ , \qquad (3)$$

with $u(\Phi_\tau)$ being a damping function of the type

$$u(\Phi_\tau) = \frac{1}{2}\left(1 + \tanh\left[\gamma_\tau(\Phi_\tau - \Phi_\tau^\circ)\right]\right) \qquad (4)$$

(because of the symmetry of the system we assign the same values 50 and 75° for γ and Φ° and whenever possible we drop the subscript τ). The functional representation given to the ROBO potential in HYBO coordinates is:

$$V^{\mathrm{ROBO}}(\rho, \alpha, \Phi) = a_1(\alpha, \Phi)\left[2\frac{\rho}{a_2(\alpha, \Phi)} - \frac{\rho^2}{a_2^2(\alpha, \Phi)}\right] \qquad (5)$$

where $a_1(\alpha, \Phi)$ describes the dependence of the well depth of the fixed Φ minimum energy path (MEP) of the exchange process, while the function $a_2(\alpha, \Phi)$ describes the location on ρ of the minimum of the fixed Φ MEP of the exchange process.

To make the LAGROBO functional form reproduce both the regions of the ab initio potential energy values bearing a single and a double barrier MEP, as in Ref. [7] the a_1 function was given the formulation

$$\begin{aligned} a_1(\alpha, \Phi) = & -D_{\mathrm{N}_2} + b_{10}(\Phi) + b_{12}(\Phi)(\alpha - 45^\circ)^2 \\ & + \left(\frac{-b_{10}(\Phi) - b_{12}(\Phi)\ (45^\circ)^2}{(45^\circ)^4}\right)(\alpha - 45^\circ)^4 \ , \end{aligned} \qquad (6)$$

where

$$b_{10}(\Phi) = c_{100} + c_{102}(\Phi - 118.6^\circ)^2 + c_{103}(\Phi - 118.6^\circ)^3 \qquad (7)$$

and

$$b_{12}(\Phi) = c_{120} + c_{121}\Phi + c_{122}\Phi^2 \ , \tag{8}$$

while the a_2 function was given the formulation

$$\begin{aligned} a_2(\alpha,\Phi) = {} & b_{20}(\Phi) + b_{22}(\Phi)(\alpha - 45^\circ)^2 \\ & + \left(\frac{3 - 3\ b_{20}(\Phi) - 2\ b_{22}(\Phi)\ (45^\circ)^2}{(45^\circ)^4} \right) (\alpha - 45^\circ)^4 \\ & + \left(\frac{-2 + 2\ b_{20}(\Phi) + b_{22}(\Phi)\ (45^\circ)^2}{(45^\circ)^6} \right) (\alpha - 45^\circ)^6 \ , \end{aligned} \tag{9}$$

where

$$b_{20}(\Phi) = c_{200} + c_{201}\Phi + c_{202}\Phi^2 + c_{203}\Phi^3 \tag{10}$$

and

$$b_{22}(\Phi) = c_{220} + c_{221}\Phi + c_{222}\Phi^2 \ . \tag{11}$$

As apparent from the formulation given above the symmetry of the system is reflected by the expansion in $\alpha - 45^\circ$ while the transition state angle is 118.6° and has an energy of 1.45 eV. Thanks to this formulation of the LAGROBO potential all the parameters of the ML4LJ PES take the same values of those of Ref. [7] except c_{100} (that quantifies the height of the C_{2v} well above the N + N_2 asymptote) that was given the value of 1.45 eV.

The key features of the strong interaction region of the ML4LJ PES are illustrated in the third column of Table 1, where the geometry and the potential energy V of the system at the reaction saddles (labeled by s) and at the bottom of the intermediate well (labeled by w) of the MEP are reported. For comparison the corresponding values of the WSHDSP and the L4 PESs are also shown.

2.2 The Empirical Long Range Attractive Tail

A first attempt to add a long range tail to the L4 PES was reported in Ref. [17]. It consisted in switching at long range from the LAGROBO to a more appropriate functional form, as done for the WSHDSP PES where the long range tail of Ref. [18] was added. More in detail, the long range attractive tail was expressed

Table 1. Key features of the reaction channels of the potential energy surfaces of N + N_2 ("s" stands for saddle, "w" for well). The geometry of the second saddle (the well is sandwiched by two symmetric barriers) is obtained by switching the values of r_{12} and r_{23} for the saddle reported.

	WSHDSP		L4		ML4LJ	
	s	w	s	w	s	w
r_{12}/bohr	2.23	2.40	2.24	2.40	2.23	2.40
r_{23}/bohr	2.80	2.40	2.77	2.40	2.82	2.40
Φ/degrees	119	120	116.7	118.6	116.4	118.6
V/eV	2.05	1.89	2.06	1.93	1.60	1.45

in terms of a linear combination of R^{-n} terms ($n = 6, 8, 10, 12$) with R being the atom diatom distance. The dependence of the related coefficients on the angle γ formed by R with the diatom internuclear distance r was expressed in terms of Legendre polynomials, while no dependence on r was assumed (as in Ref. [18]). To smoothly connect the short range behaviour to the long range one, the R^{-n} terms were scaled at $R = 4$ bohr to reproduce the L4 value, with the switch from L4 to R^{-n} being performed in an interval of about 1 bohr.

For the ML4LJ PES, instead, the functional representation of the Improved Lennard-Jones (ILJ) [19] model was adopted at long range. The ILJ potential model has the general form

$$V(R,\gamma) = \varepsilon(\gamma)\left[\frac{6}{n(R,\gamma)-6}\left(\frac{R_{\rm m}(\gamma)}{R}\right)^{n(R,\gamma)} - \frac{n(R,\gamma)}{n(R,\gamma)-6}\left(\frac{R_{\rm m}(\gamma)}{R}\right)^{6}\right] \ , \tag{12}$$

where $\varepsilon(\gamma)$ and $R_{\rm m}(\gamma)$ represent, respectively, the depth of the van der Waals potential well and its location in R. In (12), the first term describes the R-dependence of the repulsion, while the second one represents the R-dependence of the long-range attraction. The $n(R,\gamma)$ term depends on R as

$$n(R,\gamma) = \beta + 4.0\left(\frac{R}{R_{\rm m}(\gamma)}\right)^2 \ , \tag{13}$$

where β is a factor related to the hardness of the two interacting partners and is expected to vary in a limited range when passing from one system to another, bearing a specific trend. If n is assumed to be independent of R, (12) becomes identical to the usual LJ(n,6) model.

For all values of the orientation angle γ, the potential parameters are defined as

$$\begin{aligned} R_{\rm m}(\gamma) &= R_{\rm m\parallel}\cos^2\gamma + R_{\rm m\perp}\sin^2\gamma \ , \\ \varepsilon(\gamma) &= \varepsilon_{\parallel}\cos^2\gamma + \varepsilon_{\perp}\sin^2\gamma \ . \end{aligned} \tag{14}$$

The values β, $R_{\rm m\parallel}$, $R_{\rm m\perp}$, $\varepsilon_{\parallel}$ and $\varepsilon_{\perp}$ (given in Table 2) have been obtained following the guidelines reported in Refs. [19,20,21,22,23].

In Fig. 1 the energy profile of the ILJ model potential calculated for different values of γ is plotted as a function of R. As shown in the figure the profile lowers in energy at short range in moving from collinear ($\gamma = 0°$) to perpendicular ($\gamma = 90°$) approaches. On the contrary, the long range tail becomes less attractive in the same interval of γ values.

3 The Computational Machinery

The computational machinery adopted for the present study follows that of GEMS [24]. In other words, the computational procedure carries out first the ab initio calculation of the electronic energy at a properly chosen grid of molecular geometries, then fits the calculated potential energy values to a suitable functional form and integrates on it the equations of motion in their quantum version

Table 2. Empirical parameters for the ILJ long range attractive tail

β	8.2
$\varepsilon_{\parallel}$/meV	5.81
$R_{\mathrm{m}\parallel}$/bohr	7.710
$\varepsilon_{\perp}$/meV	9.77
$R_{\mathrm{m}\perp}$/bohr	6.763

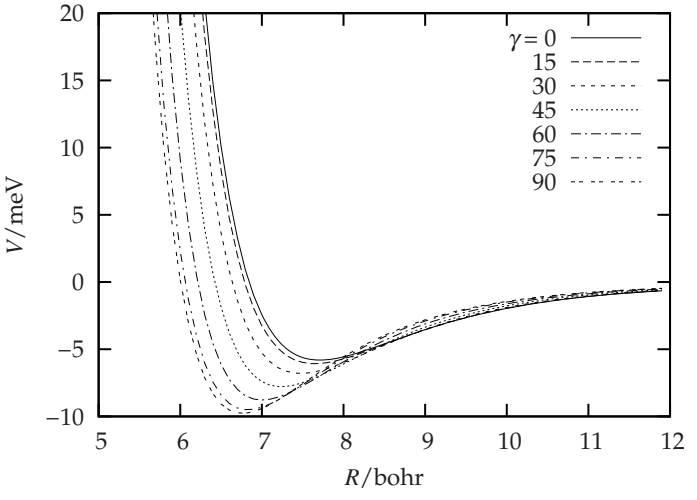

Fig. 1. Energy profile of the ILJ potential plotted as a function of the atom-diatom coordinate R for various values of the orientation angle γ, at the equilibrium diatomic internuclear distance r

to determine the relevant scattering **S** matrix (the probability **P** matrix elements are the square moduli of those of **S**). The last step consists in averaging over the unobserved variables to assemble out of the state to state **S** matrix elements the ab initio estimates of the relevant experimental observables like the thermal rate coefficient reported in this paper.

3.1 The Calculation of Detailed Quantum Probabilities

For the evaluation of quantum detailed reaction probabilities use was made of the program ABC [10], based on a time independent hyperspherical coordinate method. ABC integrates the atom-diatom Schrödinger equation for all the reactant states of a given total energy E and a fixed value of the total angular momentum (**J**) quantum number J (see Ref. [25] for more details). To this end, ABC expands the fixed E nuclei wavefunction ψ in terms of the hyperspherical arrangement channel (τ) basis functions $B^{JM}_{\tau v_\tau j_\tau K_\tau}$ labeled after J, M and K_τ (the space- and body-fixed projections of the total angular momentum **J**), v_τ and j_τ (the τ asymptotic vibrational and rotational quantum numbers), and depending on both the three Euler angles and the internal Delves hyperspherical angles. In order to carry out the fixed E and J propagation of the solution from

small to asymptotic values of hyperradius ρ (not to be confused with the ρ of the HYBO coordinates defined in (2) since ρ is now defined as $\rho = (R_\tau^2 + r_\tau^2)^{1/2}$) one needs to integrate the equations

$$\frac{\mathrm{d}^2\mathbf{g}(\rho)}{\mathrm{d}\rho^2} = \mathbf{O}^{-1}\mathbf{U}\mathbf{g}(\rho) \ . \tag{15}$$

In (15) $\mathbf{g}(\rho)$ is the matrix of the coefficients of the expansion of ψ, $\mathbf{O}$ is the overlap matrix and $\mathbf{U}$ is the coupling matrix defined as

$$U^{\tau' v'_\tau j'_\tau K'_\tau}_{\tau v_\tau j_\tau K_\tau} = \langle B^{JM}_{\tau v_\tau j_\tau K_\tau} | \frac{2\mu}{\hbar^2}(\bar{H} - E) - \frac{1}{4\rho^2} | B^{JM}_{\tau' v'_\tau j'_\tau K'_\tau} \rangle \ , \tag{16}$$

with μ being the reduced mass of the system and $\bar{H}$ the set of terms of the Hamiltonian operator not containing derivatives with respect to ρ. In ABC the integration of (15) is performed by segmenting the ρ interval into several ρ sectors inside each and through which the solution matrix is propagated from the ρ origin to its asymptotic value where the $\mathbf{S}$ matrix is determined [26]. This fixed E and J calculation is recursive and represents, therefore, the basic computational grain of the ABC program to iterate when computing the state specific probabilities and the thermal rate coefficient.

Actually, because of the large number of involved partial waves associated with the heavy mass of N + N_2 when dealing with the calculation of the rate coefficient, the approximation of evaluating the reactive probabilities associated with $J \neq 0$ by adopting the popular J-shifting model [27,28] was introduced. More in detail, in the J-shifting model the non zero J probabilities are approximated by properly shifting in energy the $J = 0$ ones ($P^{J=0}(E)$) as follows:

$$P^{JK}(E) = P^{J=0}(E - \Delta E^{JK}) \ , \tag{17}$$

with ΔE^{JK} being defined as

$$\Delta E^{JK} = \bar{B} J(J+1) + (A - \bar{B}) K^2 \ . \tag{18}$$

This formula is based on the approximation that the geometry of the system at the bent saddle is a symmetric top one. In (18) $\bar{B} = (B + C)/2$ with A, B and C being the three rotational constants of the triatom at the saddle. In the J-shifting approximation the thermal rate coefficient is in fact written as

$$k(T) = \frac{1}{hQ_\mathrm{R}} \sum_{J=0}^{\infty} (2J+1) \sum_{K=-J}^{J} \int_0^\infty e^{-E/k_\mathrm{B}T} \sum_{v,j} \sum_{v',j'} P^{J=0}_{vj \to v'j'}(E - \Delta E^{JK}) \, \mathrm{d}E \ , \tag{19}$$

where h is Planck's constant and Q_R is the total atom-diatom partition function of the reactants at temperature T per volume unit defined as

$$Q_\mathrm{R} = \left(\frac{2\pi\mu_{\mathrm{N,N_2}} k_\mathrm{B} T}{h^2} \right)^{3/2} \left(\sum_{v,j} (2j+1) e^{-\epsilon_{vj}/k_\mathrm{B}T} \right) \ , \tag{20}$$

with k_B being the Boltzmann constant.

3.2 The Computing Grid Distribution Model

As already mentioned, the present study was made possible by an intensive exploitation of the Grid to calculate single E, single J **S** matrix elements for the N + N_2 reaction. A general scheme for the concurrent reorganization of the related computer programs on the Grid is the following: a distribution procedure iterates over the E, J pairs to perform the recursive integration of (15). Accordingly, the computation is articulated as a coarse grained uncoupled loop and its distributed execution model is typical of the "parameter sweeping" type. To this end, a procedure able to handle large sets of jobs was developed. Each job execution requires the sending to the Grid of an execution script, of a specific input file and of the ABC scattering program. The execution script is the same for all jobs while the input file is different for each job. In order to better cope with the heterogeneous nature of both the computing hardware and software (compilers, libraries, submission systems, etc.) of the Grid, executable rather than source programs were distributed over the net. In fact, in spite of the fact that the time required for sending the source code is considerably shorter than that required for sending its executable (this procedure is also more selective in terms of the type of machine to adopt) this approach exploits the fact that there is no need for identifying the compiler of each machine, selecting the optimal options for compilation, compiling the code and verifying that all runs give exactly the same results as the ones obtained on the original machine.

In this work, only $J = 0$ calculations were performed: 160 single energy calculations were run concurrently in clusters of 10, thus gaining a speedup of about 16 (the overhead related to the Grid handling of the jobs is negligible with respect to the execution time of each cluster (on the average 34 hours)).

4 Results and Conclusions

As already mentioned, an extended campaign of calculations was performed at null total angular momentum for a fine grid of total energy values (energy was varied from 1.6 eV to 3.2 eV in steps of 0.01 eV). The hyperradius was varied up to 12.0 bohr and divided into 150 sectors. Basis functions with internal energy below 4.0 eV and maximum rotational quantum number 90 were all considered for the expansion.

4.1 Detailed Probabilities

For illustrative purpose we plot in Fig. 2 the state specific reactive probabilities calculated at $v = 0$ and $j = 0$ on the L4 and the ML4LJ PES. As already mentioned the ML4LJ PES was obtained by lowering the energy profile of the L4 PES (thus obtaining a ML4 PES) and adding an ILJ attractive tail. We also plot the probabilities calculated for the ML4 PES, where the long range attractive tail is not taken into account. As apparent from the figure, while the variation of the MEP in going from L4 to ML4LJ varies substantially the threshold though

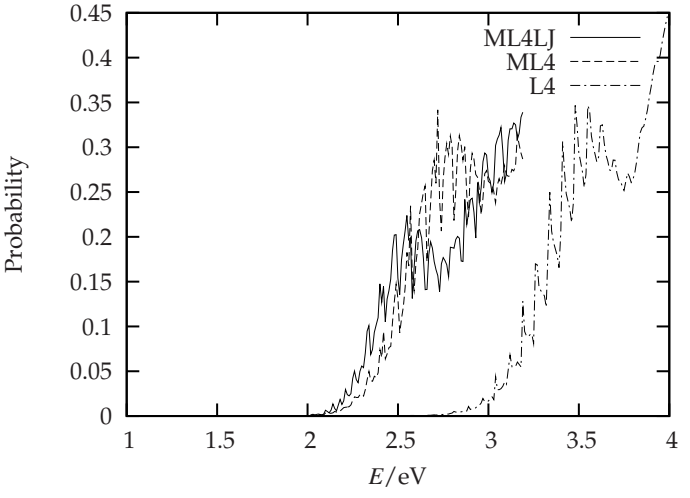

Fig. 2. Ground state specific reaction probabilities calculated on the ML4LJ (solid line), ML4 (dashed line) and L4 (dashed-dotted line) potential energy surfaces plotted as a function of total energy

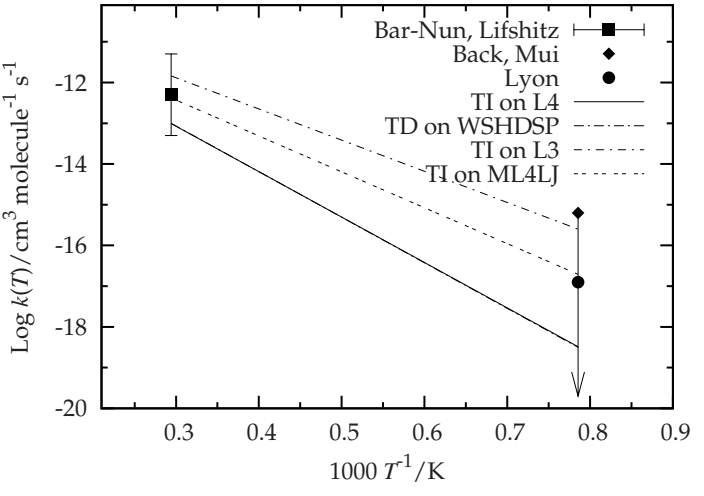

Fig. 3. Logarithm of the J-shifting rate coefficient calculated for the exchange N + N_2 reaction on the ML4LJ (dashed line), L3 (dashed-dotted line), L4 and WSHDSP (solid and dashed-dotted superimposed lines) PESs plotted as a function of the inverse temperature. The ML4LJ, L3 and L4 values were calculated with the time independent (TI) ABC program, while the WSHDSP values were obtained with a time dependent (TD) technique and reported in Ref.[6]. Experimental data of Refs. [3,4,5] are also shown. Note that the two experiments performed at $T = 1273$ K only give upper limits for the rate coefficient.

preserving the detailed structure of the state specific probabilities, adding a long range attractive tail does not vary the threshold yet enhances the low energy reactivity (as previously found for the L4 and L4w PESs of Ref. [17]). If the MEP shape is left unchanged, the resonant structure is preserved.

4.2 Thermal Rate Coefficients

The values of the thermal rate coefficients of the N + N_2 reaction calculated at the temperatures of the experiment (1273 K and 3400 K [3,4,5]) on the L3 [29], L4, WSHDSP and the present PES (ML4LJ) are shown in Fig. 3 (the values calculated on the ML4 are not shown here because they do not appreciably differ from those calculated on the ML4LJ PES). Note that the L4 and WSHDSP (solid and dahsed-dotted, respectively, superimposed lines) results underestimate the experimental values. The ML4LJ results give instead a larger value of the rate coefficient well in line with the lowering of the MEP and a better agreement with the experimental data. However, one has to be cautious in using this alignment to accredit ML4LJ as the best available PES since similar improvements could be obtained in other ways and the comparison with the experiment relies on the J-shifting approximation whose validity has still to be assessed.

Acknowledgments

Partial financial support from EGEE III, COST (D37 Gridchem), ESA ESTEC Contract 21790/08/NL/HE, ARPA Umbria, MICINN (CTQ2008-02578/BQU) and MIUR is acknowledged.

References

1. Armenise, I., Capitelli, M., Celiberto, R., Colonna, G., Gorse, C., Laganà, A.: The effect of N+N_2 collisions on the non-equilibrium vibrational distributions of nitrogen under reentry conditions. Chemical Physics Letters 227, 157–163 (1994)
2. Armenise, I., Capitelli, M., Garcia, E., Gorse, C., Laganà, A., Longo, S.: Deactivation dynamics of vibrationally excited nitrogen molecules by nitrogen atoms. effects on non-equilibrium vibrational distribution and dissociation rates of nitrogen under electrical discharges. Chemical Physics Letters 200, 597–604 (1992)
3. Back, R.A., Mui, J.Y.P.: The reactions of active nitrogen with $N^{15}O$ and N_2^{15}. Journal of Physical Chemistry
4. Bar-Nun, A., Lifshitz, A.: Kinetics of the homogeneous exchange reaction: $^{14-14}N_2$ + $^{15-15}N_2$ → 2 $^{14-15}N_2$. single-pulse shock-tube studies. Journal of Chemical Physics 47, 2878–2888 (1967)
5. Lyon, R.: Search for the N-N_2 exchange reaction. Canadian Journal of Chemistry 50, 1433–1437 (1972)
6. Wang, D., Stallcop, J.R., Huo, W.M., Dateo, C.E., Schwenke, D.W., Partridge, H.: Quantal study of the exchange reaction for N + N_2 using an ab initio potential energy surface. Journal of Chemical Physics 118, 2186–2189 (2003)
7. Garcia, E., Saracibar, A., Gómez Carrasco, S., Laganà, A.: Modeling the global potential energy surface of the N + N_2 reaction from ab initio data. Physical Chemistry Chemical Physics 10, 2552–2558 (2008)

8. Laganà, A.: A rotating bond order formulation of the atom diatom potential energy surface. Journal of Chemical Physics 95, 2216–2217 (1991)
9. Laganà, A., Ferraro, G., Garcia, E., Gervasi, O., Ottavi, A.: Potential energy representations in the bond order space. Chemical Physics 168, 341–348 (1992)
10. Skouteris, D., Castillo, J.F., Manolopoulos, D.E.: ABC: a quantum reactive scattering program. Computer Physics Communications 133, 128–135 (2000)
11. EGEE: Enabling grids for e-science in europe, `http://www.eu-egee.org`
12. Laganà, A., Riganelli, A., Gervasi, O.: On the Structuring of the Computational Chemistry Virtual Organization COMPCHEM. In: Gavrilova, M.L., Gervasi, O., Kumar, V., Tan, C.J.K., Taniar, D., Laganà, A., Mun, Y., Choo, H. (eds.) ICCSA 2006. LNCS, vol. 3980, pp. 665–674. Springer, Heidelberg (2006)
13. Laganà, A., Garcia, E., Ciccarelli, L.: Deactivation of vibrationally excited nitrogen molecules by collision with nitrogen atoms. Journal of Physical Chemistry 91, 312–314 (1987)
14. Petrongolo, C.: MRD-CI ground state geometry and vertical spectrum of N_3. Journal of Molecular Structure 175, 215–220 (1988)
15. Petrongolo, C.: MRD-CI quartet potential surfaces for the collinear reactions N (^4S_u) + N_2 ($X^1\Sigma_g^+$, $A^3\Sigma_u^+$, and $B^3\Pi_g$). Journal of Molecular Structure (Teochem) 202, 135–142 (1989)
16. Garcia, E., Laganà, A.: The largest angle generalization of the rotating bond order potential: the H + H_2 and N + N_2 reactions. Journal of Chemical Physics 103, 5410–5416 (1995)
17. Rampino, S., Skouteris, D., Laganà, A., Garcia, E., Saracibar, A.: A comparison of the quantum state-specific efficiency of N + N_2 reaction computed on different potential energy surfaces. Physical Chemistry Chemical Physics 11, 1752–1757 (2009)
18. Stallcop, J.R., Partridge, H., Levin, E.: Effective potential energies and transport cross sections for atom-molecule interactions of nitrogen and oxygen. Physical Review A 64, 042722–1–12 (2001)
19. Pirani, F., Brizi, S., Roncaratti, L.F., Casavecchia, P., Cappelletti, D., Vecchiocattivi, F.: Beyond the Lennard-Jones model: a simple and accurate potential function probed by highly resolution scattering data useful for molecular dynamics simulations. Physical Chemistry Chemical Physics 10, 5489–5503 (2008)
20. Cambi, R., Cappelletti, D., Liuti, G., Pirani, F.: Generalized correlations in terms of polarizability for van der waals interaction potential parameter calculations. Journal of Chemical Physics 95, 1852–1861 (1991)
21. Pirani, F., Cappelletti, D., Liuti, G.: Range, strength and anisotropy of intermolecular forces in atom-molecule systems: an atom-bond pairwise additivity approach. Chemical Physics Letters 350, 286–296 (2001)
22. Capitelli, M., Cappelletti, D., Colonna, G., Gorse, C., Laricchiuta, A., Liuti, G., Longo, S., Pirani, F.: On the possibility of using model potentials for collision integral calculations of interest for planetary atmospheres. Chemical Physics 338, 62–68 (2007)
23. Cappelletti, D., Pirani, F., Bussery-Honvault, B., Gomez, L., Bartolomei, M.: A bond-bond description of the intermolecular interaction energy: the case of weakly bound N_2-H_2 and N_2-N_2 complexes. Physical Chemistry Chemical Physics 10, 4281–4293 (2008)
24. Laganà, A.: Towards a grid based universal molecular simulator. In: Theory of the dynamics of elementary chemical reactions, pp. 363–380. Kluwer, Dordrecht (2004)
25. Schatz, G.C.: Quantum reactive scattering using hyperspherical coordinates: results for H + H_2 and Cl + HCl. Chemical Physics Letters 150, 92–98 (1988)

26. Pack, R.T., Parker, G.A.: Quantum reactive scattering in three dimensions using hyper-spherical (APH) coordinates. theory. Journal of Chemical Physics 87, 3888–3921 (1987)
27. Bowman, J.M.: Reduced dimensionality theory of quantum reactive scattering. Journal of Physical Chemistry 95, 4960–4968 (1991)
28. Bowman, J.M.: Approximate time independent methods for polyatomic reactions. Lecture Notes in Chemistry 75, 101–114 (2000)
29. Laganà, A., Faginas Lago, N., Rampino, S., Huarte-Larrañaga, F., Garcia, E.: Thermal rate coefficients in collinear versus bent transition state reactions: the N + N_2 case study. Physica Scripta 78, 058116–1–9 (2008)